Available online at www.sciencedirect.com

ScienceDirect

Geochimica et Cosmochimica Acta 269 (2020) 292–302

Geochimica et Cosmochimica Acta

www.elsevier.com/locate/gca

Predicting equilibrium intramolecular isotope distribution within a large organic molecule by the cutoff calculation

Yuyang He [a,b,*], Huiming Bao [b,c], Yun Liu [c,d]

[a] Institute of Mechanics, Chinese Academy of Sciences, No. 15 Beisihuanxi Road, Beijing 100190, China
[b] Department of Geology and Geophysics, Louisiana State University, E235 Howe Russell Kniffen, Baton Rouge, LA 70803, United States
[c] Institute of Geochemistry, Chinese Academy of Sciences, Guiyang 550081, China
[d] CAS Center for Excellence in Comparative Planetology, Hefei 230026, China

Received 9 April 2019; accepted in revised form 23 October 2019; available online 2 November 2019

Abstract

A predicted equilibrium intramolecular isotope distribution (Intra-ID) serves as a reference for measured position-specific (PS) isotope composition variation in an organic molecule. Equilibrium Intra-ID can be estimated from calculated reduced partition function ratios (RPFR or β factor), which are largely absent to date. For relatively small molecules, the PS β factor can be calculated directly. However, estimating the PS β factor considering an entire, large organic molecule is computationally prohibitive. The isotope effect is local in that the vibrational frequencies of an atom are only affected by its proximal bonding environment. Therefore, the cutoff calculation, which simplifies the calculation of an entire molecule to a local area, was previously proposed for large organic molecules. However, the cutoff size was not validated, which has hindered the application of the cutoff calculation. Here, we calculated a series of small organic molecules with 2–18 carbon atoms to test the influence of cutoff size on the $^{13}\beta$ value estimation of a target carbon position in a carbon chain or a carbon ring. We calculated nineteen small molecules that have a methyl carbon and a functional group that is at least three bonds away from the target methyl position. The result showed that the equilibrium ^{13}C enrichment of the methyl group relative to CO_2 at 25 °C ($\ln^{13}\alpha_{(eq)}$) for the nineteen molecules varied in a small range, with a standard deviation of 0.2‰. Fourteen aromatic hydrocarbons with a benzene and one adjacent functional group were calculated to test the influence of different adjacent functional groups on similar carbon positions in benzene. The results showed that different adjacent functional groups had significant influence only on the predicted $\ln^{13}\alpha_{(eq)}$ value of the carbon position directly connected to them (standard deviation = 1.0‰, n = 14), with a negligible influence on the predicted $\ln^{13}\alpha_{(eq)}$ value of the remaining carbons in benzene (standard deviation = 0.2‰, n = 14). The PS $^{13}\beta$ value of a specific carbon position in CoA calculated by the cutoff calculation differed from that of the entire-molecule calculation by 0.0–0.3‰. We concluded that the cutoff calculation simplified the calculation of a target position from an entire molecule to a cluster of three proximal bonds in a chain and/ or an adjacent ring, providing PS $^{13}\beta$ values of sufficient accuracy for large organic molecules.

Keywords: Reduced partition function ratio; Position-specific isotope composition; KIE; Solvent effect; CoA

1. INTRODUCTION

A large organic molecule has multiple elements, such as carbon or hydrogen, and each element has many different positions within a molecule. Since Abelson and Hoering (1961) first isolated and measured $\delta^{13}C$ values of carboxyl

* Corresponding author at: Institute of Mechanics, Chinese Academy of Sciences, No. 15 Beisihuanxi Road, Beijing 100190, China.
E-mail address: yhe@imech.ac.cn (Y. He).

https://doi.org/10.1016/j.gca.2019.10.032
0016-7037/

carbons in amino acids, an increasing number of position-specific (PS) $\delta^{13}C$ have been measured by pioneers using analytical approaches such as chemical degradation (Rinaldi et al., 1974; Monson and Hayes, 1980, 1982; Rossmann et al., 1991; Gleixner and Schmidt, 1997; Savidge and Blair, 2004, 2005) or pyrolysis (Corso and Brenna, 1997; Oba and Naraoka, 2006). In recent years, using gas-chromatography-pyrolysis/combustion-isotope ratio mass spectrometry (Gilbert et al., 2016a, 2016b, 2019; Nimmanwudipong et al., 2015; Piasecki et al., 2016a, 2018; Suda et al., 2017; Li et al., 2018), flow-injection analysis-reaction-isotope ratio mass spectrometry (Fry et al., 2018), orbitrap mass spectrometry (Eiler et al., 2017), or isotopic ^{13}C nuclear magnetic resonance spectroscopy (Bayle et al., 2014, 2015; Diomande et al., 2015; Gilbert et al., 2009; 2010, 2011a, 2011b, 2012a, 2012b; Joubert et al., 2018; Julien et al., 2015a, 2015b, 2016; Romek et al., 2016; Remaud and Akoka, 2017; Robins et al., 2017; Liu et al., 2018, 2019), researchers are actively developing techniques for $\delta^{13}C$ position-specific isotope analysis (PSIA). The measured or predicted PS isotope composition distribution within a molecule is called intramolecular isotope distribution (Intra-ID). Intra-ID contains information about carbon source, reaction pathways, and their associated equilibrium or kinetic isotope effects (EIE or KIE), which is concealed or lost in bulk molecule isotope compositions.

Intra-ID has become a promising tool for identifying and quantifying the production and consumption pathways of large molecules. The study of PS $\delta^{13}C$ values of carboxyl carbons in amino acids suggested that CO_2 fixation could occur via the citric acid cycle in addition to the ribulose diphosphate pathway in photosynthesizing algae (Abelson and Hoering, 1961). Different fatty acid Intra-ID in *E. coli* and *S. cerevisiae* revealed different fatty acid metabolic and catabolic processes (Monson and Hayes, 1980, 1982). Analysis of propane produced from different pathways showed that Intra-ID of propane produced from anaerobic bacterial oxidation has ^{13}C enriched in the central position, which is different from that in the thermogenic propane (Gilbert et al., 2019). In addition, propane Intra-ID is a promising geothermometer (Webb and Miller III, 2014; Gilbert et al., 2016a, 2019; Piasecki et al., 2016a, 2016b, 2018; Eiler et al., 2018; Li et al., 2018; Liu et al., 2018; Xie et al., 2018). Intra-ID can serve as forensic evidence to discriminate the precursors of organic molecules (Meinschein et al., 1974; Gilbert et al., 2012a, 2012b; Julien et al., 2016). It has also been used to study the volatilization process of organic compounds, such as methanol, toluene, and bromothane (Julien et al., 2015a, 2015b).

It has been observed that reversible biochemical reactions exist, which has the potential to reach local isotope equilibrium (ap Rees and Morrell, 1990; Igamberdiev and Kleczkowski, 2009, 2011; Morandini, 2009). The combination of reversible and irreversible reactions can lead an organism to different sets of steady-state. While many factors can result in various sets of disequilibrium in Intra-IDs, to quantify a set of disequilibrium state, we need a reference, and the intramolecular equilibrium state is such a reference. The reduced partition function ratio (RPFR or β factor) is the equilibrium isotope fractionation factor between a PS atom in a molecule and its atomic form. Galimov pointed out the similarity between measured $\delta^{13}C$ values and his predicted $^{13}\beta$ values in molecules such as acetoin, malate, and chlorophyll. He proposed that such similarity should be used as a fingerprint for the existence of reversible biochemical reactions that lead biomolecules to reach a close-to-equilibrium steady-state (Galimov, 1985, 2004, 2006). The calculated EIEs can also assist and improve our understanding and interpretation of experimental and field KIE observations (Bennet and Sinnott, 1986; Chen et al., 2000a, 2000b; Williams and Wilson, 2016; He et al., 2018).

PSIA is available for some large molecules, such as sucrose (Gilbert et al., 2012b), long chain n-alkane (Gilbert et al., 2013), and nicotine (Romek et al., 2016), and will predictably be available for even more complex biomolecules, such as proteins and DNA, in the coming years. We have few theoretical predictions of equilibrium Intra-IDs, since the theoretical calculation for large organic molecules is computational prohibitive. Such computational limitations have hindered our understanding and widespread application of Intra-ID.

β values can be calculated theoretically. However, the KIE and EIE calculations for large molecules are time-consuming and are limited by the molecular size. For a molecule with n atoms, the current computational time increases approximately proportional to n^3 (Stern and Wolfsberg, 1966b) or n^4 (Rustad, 2009). In addition, to obtain more accurate results, higher theoretical levels are needed. For instance, when computing β values under supercold conditions, we must consider the Born-Oppenheimer correction for light elements such as C, H, O, and N. Such calculation requires the use of second-order Møller-Plesset (MP2) perturbation theory with the aug-cc-pVTZ basis set (Zhang and Liu, 2018). However, for a molecule with 13–27 atoms, the CPU time taken by MP2 calculations are 3–11 times that of Density Functional Theory (DFT) calculations, which is also proportional to the number of atoms in a molecule (Rustad, 2009). Therefore, the calculation of large molecular size with high theoretical levels is even more restricted by current computer powers.

Considerable effort has been devoted to simplifying the computation of isotope effects for large molecules. A theoretical derivation showed that the EIE and KIE calculations of a target atom can be simplified by considering vibrational frequencies of bonds in a local area (Herschbach et al., 1959). Another preliminary investigation also showed that at room temperature and above, calculated compound-specific KIEs of a reaction do not differ significantly between considering an entire molecule and considering only the neighbor atoms close to the reaction site (Wolfsberg and Stern, 1964; Stern and Wolfsberg, 1966b). The simplification approach that considers only the closest surroundings is termed the "cutoff" calculation (Wolfsberg and Stern, 1964; Stern and Wolfsberg, 1966a, 1966b). The cutoff calculation was applied to H/D isotopes during the early years of stable isotope effect research. The

H/D KIE calculation was simplified by considering only three to five collinear atoms (Sharp and Johnston, 1962). The calculation of simple molecule reactions showed that H/D fractionation depends significantly on the directly linked carbons, which validated the cutoff calculation (Hartshorn and Shiner Jr, 1972). The cutoff approach is promising for calculating EIE and KIE of large molecule systems. However, compared to experimental results, the accuracy of such simplification is "open to grave doubt" (Sharp and Johnston, 1962) and should not be "tacitly accepted" (Wolfsberg and Stern, 1964; Stern and Wolfsberg, 1966b) without necessary calculation tests.

Galimov developed a generalized semiempirical approach to estimate PS $^{13}\beta$ factor from isotopic bond numbers (L_j) of a target carbon atom ($^{13}\beta = 1 + \sum_{j=1}^{n} L_j$). L_j is a numerical value that quantifies chemical bond types (Galimov, 1985). Such an approach successfully predicted that the carboxyl carbon would be preferentially enriched in ^{13}C over other carbon positions in amino acids, which has been confirmed by experiments (Abelson and Hoering, 1961; Gilbert et al., 2011a, 2013; Monson and Hayes, 1980, 1982; Robins et al., 2017; Romek et al., 2016). Galimov's approach offers an efficient but not very accurate approximation for many carbon positions in organic compounds. The reason is that the PS $^{13}\beta$ factor of an atom is determined not only by its bond types but also by its adjacent functional groups.

Ab initio calculation reliably estimates the β factor theoretically. Using MP2 and DFT methods, Rustad calculated the average and PS $^{13}\beta$ values for carbons in 20 standard amino acids (Rustad, 2009). The calculation results agree with Galimov's prediction that the carboxyl carbon would be heavier than other carbons in amino acids at equilibrium. However, in Galimov's method, the $^{13}\beta$ value of a carbon position was calculated by considering only its direct bonds. For instance, two carboxyl carbons in different amino acids would have the same $^{13}\beta$ values even if the attached carbon groups were different. Rustad's calculation illustrated that the $^{13}\beta$ values of the same positions are similar but vary in different molecules. For instance, the $^{13}\beta$ values of carboxyl carbons can differ by as much as 5‰ between isoleucine and asparagine; the $^{13}\beta$ values of amine carbons differ by 5.6‰ between isoleucine and threonine; the $^{13}\beta$ values of methyl carbons differ by 2.9‰ between isoleucine and threonine; and the $^{13}\beta$ values of methylene carbons differ by 7.0‰ between tryptophan and arginine. The $^{13}\beta$ values of similar positions vary even within the same molecule. For example, the methylene carbons in arginine have PS $^{13}\beta$ values ranging from –22.5‰ to –27.7‰ (Rustad, 2009).

Quantum mechanical/molecular mechanical (QM/MM) considers an active site of an enzymatic reaction that is bonded immediately to a few functional groups as its inner layer. The inner layer is calculated by the QM method. The core group is subsequently surrounded by more atoms as a background environment, which is calculated by the MM method. Based on force constants and molecular geometry obtained from the QM/MM approach, compound-specific KIEs for enzyme catalytic biochemical reactions have been calculated using, for example, the ISOEFF program (Anisimov and Paneth, 1999; Świderek and Paneth, 2011, 2012, 2013). The QM/MM approach simplifies the calculation of KIE but also compromises the calculation accuracy. In addition, for the calculation of KIE, the transition-state structure is usually searched manually until the calculated KIE agrees with experimental values. Such a method is not only cumbersome but also ineffective in providing independent evidence or predicting alternating transition-state structures (Williams and Wilson, 2016).

Recent PS $^{D}\beta$ calculation of a target hydrogen atom of a set of organic molecules showed that hydrogens on carbon chains can be approximated by a cutoff molecule with only two neighbor bonds, and hydrogens on rings can be approximated by a single ring (Wang et al., 2009a, 2009b, 2013). Thus, cutoff calculation, or cluster model, should be applicable to large molecules. However, it is necessary to reevaluate the size of the cluster that can be applied to organic molecule cutoff calculations. A variety of cluster models have been successfully applied to represent minerals or solutions and obtain β values (Liu and Tossell, 2005; Rustad et al., 2008, 2010; Li and Liu, 2011, 2015; Zhang and Liu, 2014; He and Liu, 2015; Gao et al., 2018). In these cutoff calculations, the structures are normally simplified according to the *NNN* rule, which means that the β value of a target atom can be simplified to its closest three bonds in minerals or three shells of water molecules (usually 24 water molecules) in solutions (Gao et al., 2018). We predict that the calculation of PS $^{13}\beta$ values for a target position in a large molecule can be simplified to a cluster, in which the target atom has its closest three adjacent bonds in a chain and/ or one adjacent ring. The PS $^{13}\beta$ value estimated by the cutoff calculation should be within a small error range of those calculated by the tedious or often improbable entire-molecule calculation.

DFT with the B3LYP exchange-correlation function has been routinely used in QM calculation. The validity of B3LYP with different basis sets for calculating harmonic vibrational frequencies of $^{12}CH_4$ and $^{12}C_3H_8$ isotopologues was evaluated and discussed in a previous study (Piasecki et al., 2016b). It has been used to calculate PS β values of organic molecules, such as carbon and hydrogen isotopes in small hydrocarbon molecules (Rustad, 2009; Wang et al., 2009a, 2009b, 2013; Webb and Miller III, 2014; Piasecki et al., 2016b) and Mg isotopes in chlorophyll (Black et al., 2007). Here, we use DFT with the Urey-Bigeleisen-Mayer model to calculate PS $^{13}\beta$ values at 25 °C for a set of organic molecules with 2–18 carbon atoms. The calculation results are used to test the size of the cutoff calculation for large organic molecules. Coenzyme A (CoA) plays an important role in fatty acids and pyruvate metabolism. The simplification of CoA is the key to KIE calculations of biochemical reactions for fatty acids and glucose. In addition, CoA is a relatively small enzyme with both chains and rings, which is an ideal subject to test the accuracy of the cutoff calculation. We therefore use CoA as an example to compare the $^{13}\beta$ value results of the cutoff calculation with those of the entire-molecule calculation.

2. METHOD

2.1. Cutoff calculations

The cutoff calculation uses a small molecule to represent an atom at similar positions in a large molecule. The bond being cut will leave an unsaturated atom. The volume variable cluster model (VVCM) is a widely used cluster model in mineral calculations. It uses virtual charges to balance valences and cancel volume variations that result from unbalanced valences (He and Liu, 2015, Gao et al., 2018). Similar to VVCM, in the cutoff calculation for organic molecules, we saturate the bond being cut with a hydrogen atom. Rings must be considered as a whole and cannot be cut to pieces. Each target atom is surrounded by at least three bonds in a chain or at least a ring on each side. The molecule structures are built by GaussView 5 (Semichem Inc.) software.

To examine the influence of cluster size on PS $^{13}\beta$ value estimation, we first calculated n-pentane, n-hexane, n-heptane, 3-methylpentane, 3-methylhexane, acetic acid, propionic acid, butanoic acid, pentanoic acid, and hexanoic acid. The deviation of PS $^{13}\beta$ values at carbon positions in a similar bond environment is examined by comparing similar carbon positions in normal alkanes, isomeric alkanes, and carboxylic acids.

The combinations of all functional groups are impossible to test individually. Thus, we built a set of molecules with a functional group at least three bonds away from a terminal methyl. The chosen functional groups are ketone (2-hexanone), acyl chloride (pentanoyl chloride), amine (butylamine), amine and carboxyl (2- aminopentanoic acid), alcohol (n-butanol), phosphate (n-butylphosphate), ether (butyl methyl ether), thiol (1-butanethiol), nitrile (pentanenitrile), chloride (n-butyl chloride), benzene (butylbenzene), cyclopentadiene (n-butyl cyclopentadiene), tetrahydrofuran (2-butyltetrahydrofuran), and pyrrole (n-butylpyrrole). To ensure that the terminal methyl carbons are in a similar bond environment, we put methylenes in between the methyl carbons and the functional groups. Using methyl carbon as an example, we test the influence of different functional groups that are three bonds away from the target position on PS $^{13}\beta$ value estimates.

The calculation for carbon rings takes more time than carbon chains. Thus, it is more essential to simplify carbon ring calculations. Here, we use a set of aromatic hydrocarbons to test the influence of functional groups on the PS $^{13}\beta$ values of benzene. The aromatic hydrocarbons are toluene, ethylbenzene, n-propylbenzene, n-butylbenzene, biphenyl, 2-phenyltoluene, 3-phenyltoluene, 4-phenyltoluene, diphenylmethane, bibenzyl, dibenzoylmethane, 4-phenylpyridin, 2-phenyltetrahydrofuran, and para-terphenyl. The carbons on the target benzene are called C1 for the position immediately adjacent to a functional group and C6 for the carbon the furthest away from the adjacent functional groups (Fig. 1).

The three tests set up the basis of our cutoff calculations for organic molecules. Next, we use CoA as an example to test if the choice of cluster size can be generalized to carbon positions other than methyl, methylene, carboxylic and

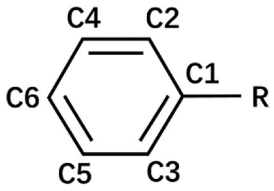

Fig. 1. Structure and named carbon numbers of benzene in aromatic hydrocarbons.

benzene carbons. The structure of the CoA is shown as cluster 0 in Fig. 2, which is optimized as an entire molecule. The structure of CoA is reduced to small clusters, where each target atom has at least three adjacent bonds in a chain and/or one adjacent ring to represent the whole structure (Fig. 2). The carbons are named C_{fli}, where f indicates the cluster number and i indicates the carbon number in the cluster.

We built cluster 1 from $C_{0/1}$-$C_{0/14}$. Cluster 1 contains an adenine ($C_5N_5H_5$, ), a $C_5H_{11}O_{13}P_3$ 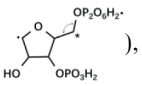), and an isobutane ) (dots are the connecting point). In cluster 1, $C_{1/1}$–$C_{1/10}$ are representative of positions $C_{0/1}$–$C_{0/10}$. Except for cluster 1, the rest of the molecule is a chain. Thus, we can simplify each position by keeping the closest 3 bonds. $C_{2/2}$–$C_{2/6}$, $C_{3/6}$, $C_{4/3}$, and $C_{5/3}$-$C_{5/6}$ are representative of $C_{0/11}$–$C_{0/15}$, $C_{0/16}$, $C_{0/17}$, and $C_{0/18}$–$C_{0/21}$, respectively (see molecule structure configurations in SI for atom numbers).

2.2. $^{13}\beta$ calculation

All optimization and harmonic vibrational frequency calculations for the ground states are performed using DFT with the B3LYP exchange-correlation function (Lee et al., 1988; Becke, 1993) and 6-311G++/d,p basis set in Gaussian 09 software (Gaussian Inc.).

Using calculated vibrational frequencies, we estimate single substituted PS $^{13}\beta$ values in harmonic approximation using the Urey-Bigeleisen-Mayer model (Bigeleisen and Mayer, 1947; Urey, 1947):

$$\beta = \prod_{i}^{3n-6} \left(\frac{u_i^*}{u_i}\right)\left(\frac{e^{-u_i^*/2}}{e^{-u_i/2}}\right)\left(\frac{1-e^{-u_i}}{1-e^{-u_i^*}}\right) \quad (1)$$

where only the most abundant isotope is considered for atoms other than the target position.

The relative equilibrium PS ^{13}C enrichment at 25 °C in position i is reported as the equilibrium fractionation value relative to gas CO_2 ($\ln {}^{13}\alpha_{eq} = \ln \frac{{}^{13}\beta_i}{{}^{13}\beta_{CO_{2(g)}}}$, calculated ${}^{13}\beta_{CO2} = 1.196457$). The $\ln {}^{13}\alpha_{eq}$ cancels some calculation errors for the absolute $^{13}\beta$ values and offers a direct and more accurate scale of the degree of isotope fractionation, which has also been adopted by Rustad (2009). Scaling factors are not considered since they are canceled in the $\ln {}^{13}\alpha_{eq}$. Here, we only compare the vibrational frequencies calculated by the cutoff calculation with those from the entire-molecule calculation. Corrections such as anharmonic

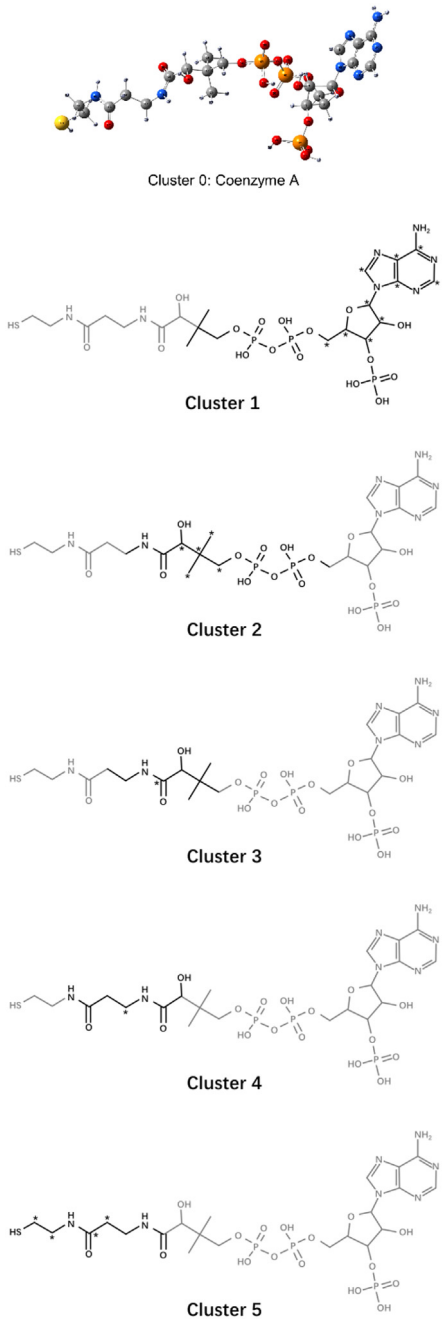

Fig. 2. Structures of Coenzyme A and five reduced clusters built for the cutoff calculation. In the configuration of CoA, gray spheres represent carbon atoms, white spheres represent hydrogen atoms, red spheres represent oxygen atoms, blue spheres represent nitrogen atoms, yellow spheres represent sulfur atoms, and orange spheres represent phosphorus atoms. For the clusters' chemical structures, black parts are the reduced cluster, and gray parts are ignored. Stars indicate target atoms. (For interpretation of the references to colour in this figure legend, the reader is referred to the web version of this article.)

and Born-Oppenheimer corrections can be later applied based on the calculation results.

To test the cutoff approach, it is necessary to examine the influence of cluster size and adjacent functional groups on the $^{13}\beta$ values of a specific position. To compare the results of calculations using different clusters for the same carbon position, we use the absolute value of $\ln {}^{13}\alpha_{i-j} = \ln \frac{{}^{13}\beta_i}{{}^{13}\beta_j}$ to represent the $^{13}\beta$ value difference in a specific position between clusters i and j.

3. RESULTS

Here, we first use normal alkanes, isomeric alkanes, and carboxylic acids to test the influence of cluster size on PS $^{13}\beta$ value estimation in carbon chains. Then, a set of chain molecules with a functional group that is at least three bonds away in a chain from a terminal methyl is used to test if the cutoff calculation can simplify the calculation of the terminal methyl to a cluster with three proximal bonds. Next, the calculation of a set of aromatic hydrocarbons is used to test the validity of the cutoff calculation for rings. Finally, we use CoA to test the accuracy of the cutoff calculation for $^{13}\beta$ values for a large molecule and see if the chain and ring simplification can be expanded to other carbon positions other than methyl, carboxyl, and benzene carbons. All the optimized structure coordinates can be found in *S1. Optimized coordinates* in SI. The PS $\ln {}^{13}\alpha_{eq}$ values of carbons in each molecule are labeled in *S2. Structures and the corresponding* $ln^{13}\alpha_{eq}$ *values* in SI.

3.1. Carbon chains

For a normal alkane, there are only three structurally-distinct bonding environments: terminal methyl (*CH_3–CH_2–CH_2–), methylene adjacent to the terminal methyl (CH_3–*CH_2–CH_2–), and methylene in between two other methylenes (–CH_2–*CH_2–CH_2–). The smallest unit that contains all three types of carbons is n-pentane. Here, we compared the same positions in n-pentane, n-hexane, and n-heptane (Table 1).

The standard deviation of the large organic molecule PSIA for $\delta^{13}C$ is ~0.1–2.7‰ (Gilbert et al., 2011a, 2013, 2016b; Romek et al., 2016). As shown in Table 1, compared with current laboratory measurement errors, the $\ln {}^{13}\alpha_{i\text{-}j}$ value differences for all the carbon positions in normal alkanes are negligible ($\ln {}^{13}\alpha_{i\text{-}j(\max)} < 0.1$‰). Extending the length of the carbon chains does not influence the predicted PS $^{13}\beta$ values in normal alkanes much.

For 3-methylpentane and 3-methyl hexane, the PS $^{13}\beta$ values of similar carbon positions are also minimally different (Table 2). The $\ln {}^{13}\alpha_{i\text{-}j}$ value of the methyl carbons next to a methylene carbon (*CH_3–CH_2–) and of the methyl carbons next to a tertiary carbon (*CH_3–CH–) between the two isomeric alkanes is 0.1‰, and the $\ln {}^{13}\alpha_{i\text{-}j}$ value between the two tertiary carbons (–*CH–) is 0.4‰.

The calculated PS $^{13}\beta$ values for carboxylic acids with 2–6 carbons are shown in Table 3. Comparing the carboxylic acids, we can see that the PS $^{13}\beta$ values of the terminal methyl carbons and carboxyl carbons are similar, with $\ln {}^{13}\alpha_{met(eq)} = -49.8 \pm 0.4$‰ and $\ln {}^{13}\alpha_{carb(eq)} = -2.4 \pm 0.1$‰, n = 5, respectively.

Next, we tested the influence of a functional group that is at least three methylenes in a chain away from a terminal

Table 1
Calculated position-specific $\ln^{13}\alpha_{eq}$ values (‰) for n-pentane, n-hexane, and n-heptane. The $\ln^{13}\alpha_{eq}$ value indicates enrichment in ^{13}C relative to $CO_{2(g)}$ at 25 °C. n is the number of $\ln^{13}\alpha_{eq}$ values that are used to calculate the standard deviation.

Molecule	Structure	*CH_3–CH_2-CH_2-	CH_3–*CH_2-CH_2–	–CH_2–*CH_2–CH_2–
n-Pentane		−50.3	−36.0	−35.0
		−50.3	−36.0	
n-Hexane		−50.4	−36.0	−35.0
		−50.4	−35.9	−35.0
n-Heptane		−50.3	−36.0	−35.1
		−50.3	−36.0	−35.1
				−35.1
Standard deviation (n = 6)		0.05	0.04	0.05

Table 2
Calculated position-specific $\ln^{13}\alpha_{eq}$ values (‰) for 3-methylpentane and 3-methylhexane. The $\ln^{13}\alpha_{eq}$ value indicates enrichment in ^{13}C relative to $CO_{2(g)}$ at 25 °C.

Molecule	Structure	*CH_3–CH_2–	CH_3–*CH_2–	–CH_2–*CH_2–CH–	–*CH–	*CH_3–CH–
3-Methylpentane		−50.4	−35.6		−25.0	−49.0
		−50.4	−35.6			
3-Methylhexane		−50.3	−36.2	−34.5	−24.6	−49.1
		−50.3	−36.2	−34.5		

Table 3
Calculated position-specific $\ln^{13}\alpha_{eq}$ values (‰) for carboxylic acids. The $\ln^{13}\alpha_{eq}$ value indicates enrichment in ^{13}C relative to $CO_{2(g)}$ at 25 °C.

Molecule	Structure	CH_3–	–CH_2–	–COOH
Acetic acid		−49.9		−2.6
Propionic acid		−48.9	−37.4	−2.2
Butanoic acid		−49.8	−34.8	−2.4
			−36.6	
Pentanoic acid		−50.0	−35.7	−2.5
			−33.9	
			−36.7	
Hexanoic acid		−50.2	−35.8	−2.4
			−34.7	
			−33.8	
			−36.6	

Table 4
Calculated position-specific $\ln^{13}\alpha_{eq}$ values (‰) for molecules with a functional group that is 3 bonds away from a terminal methyl. The $\ln^{13}\alpha_{eq}$ value indicates enrichment in ^{13}C relative to $CO_{2(g)}$ at 25 °C. n is the number of $\ln^{13}\alpha_{eq}$ values that are used to calculate the standard deviation.

Molecule	Structure	$\ln^{13}\alpha_{met(eq)}$
Pentane		−50.3
Hexane		−50.4
Heptane		−50.3
Pentanoic Acid		−50.0
Hexanoic acid		−50.2
2-Hexanone		−50.2
Pentanoyl chloride		−50.0
n-butanol		−50.2
Butylamine		−50.4
n-Butyl chloride		−50.1
1-Butanethiol		−50.1
Butyl methyl ether		−50.2
Pentanenitrile		−49.9
n-Butylphosphate		−50.0
2- Aminopentanoic acid		−50.1
n-Butyl cyclopentadiene		−50.3
n-Butylbenzene		−50.5
n-Butylpyrrole		−50.3
2-Butyltetrahydrofuran		−50.2
Standard deviation (n = 19)		0.2

methyl carbon (Table 4). The results show that the influence of a functional group on the methyl group varies within a small standard deviation ($\ln^{13}\alpha_{eq} = -50.2 \pm 0.2$‰, n = 19).

3.2. Carbon rings

The PS $^{13}\beta$ values of benzene carbons in 14 aromatic hydrocarbons are calculated (Table 5). The $\ln^{13}\alpha_{eq}$ values for the six carbons are -20.5 ± 1.0‰, -31.7 ± 0.2‰, -31.7 ± 0.2‰, -31.9 ± 0.2‰, -31.9 ± 0.2‰, and -32.3 ± 0.2‰ for C1 to C6, respectively.

3.3. Applications of cutoff calculations for CoA

Here, we use CoA to test the accuracy of the cutoff calculation for $^{13}\beta$ value estimates for a large molecule and see if the chain and ring simplification can be expanded to other carbon positions. The calculated $\ln^{13}\alpha_{eq}$ values for the entire CoA molecule and 5 clusters and their absolute differences are shown in Table 6.

Table 5
Calculated position-specific $\ln^{13}\alpha_{eq}$ values (‰) of for six-carbon benzene in different aromatic hydrocarbons. The $\ln^{13}\alpha_{eq}$ value indicates enrichment in ^{13}C relative to $CO_{2(g)}$ at 25 °C. n is the number of $\ln^{13}\alpha_{eq}$ values that are used to calculate the standard deviation.

Molecule	Structure	C1	C2	C3	C4	C5	C6
Toluene		−21.1	−31.6	−31.6	−32.0	−32.0	−32.6
Ethylbenzene		−20.1	−31.8	−31.8	−32.0	−32.0	−32.4
n-Propylbenzene		−20.1	−31.8	−31.9	−32.1	−32.1	−32.5
n-Butylbenzene		−20.3	−31.8	−31.8	−32.0	−32.0	−32.4
Biphenyl		−20.3	−31.7	−31.7	−31.9	−31.9	−32.3
2-Phenyltoluene		−19.8	−31.6	−31.9	−31.9	−31.8	−32.0
3-Phenyltoluene		−20.3	−31.8	−31.8	−31.9	−31.9	−32.3
4-Phenyltoluene		–22.6	−31.6	−31.5	−31.6	−31.6	−32.3
Diphenylmethane		−21.5	−31.7	−31.5	–32.0	−31.9	−32.4
Bibenzyl		−20.1	−31.9	−31.9	–32.1	–32.1	−32.5
Dibenzoylmethane		−20.3	−31.9	−31.9	–32.0	–32.1	−32.5
4-Phenylpyridin		−19.6	–32.1	–32.1	−31.7	−31.7	–32.0
2-Phenyltetrahydrofuran		−18.9	−31.5	−31.3	–32.0	−31.9	–32.3
para-Terphenyl		–22.6	−31.4	−31.4	−31.6	−31.6	–32.3
Standard deviation (n = 14)		1.0	0.2	0.2	0.2	0.2	0.2

Table 6
Comparison of $\ln^{13}\alpha_{eq}$ values (‰) calculated from an entire Coenzyme A molecule using the cutoff calculation. The $\ln^{13}\alpha_{eq}$ value indicates enrichment in ^{13}C relative to $CO_{2(g)}$ at 25 °C.

	Whole molecule	Cutoff calculation	Absolute difference	Whole molecule	Cutoff calculation	Absolute difference
Atom	$C_{0/1}$	$C_{1/1}$		$C_{0/12}$	$C_{2/3}$	
$\ln^{13}\alpha_{eq}$	−4.6	−4.5	0.1	−16.4	−16.6	0.2
Atom	$C_{0/2}$	$C_{1/2}$		$C_{0/13}$	$C_{2/4}$	
$\ln^{13}\alpha_{eq}$	−21.1	−21.2	0.1	−46.8	−47.0	0.2
Atom	$C_{0/3}$	$C_{1/3}$		$C_{0/14}$	$C_{2/5}$	
$\ln^{13}\alpha_{eq}$	−4.2	−4.3	0.1	−46.3	−46.2	0.1
Atom	$C_{0/4}$	$C_{1/4}$		$C_{0/15}$	$C_{2/6}$	
$\ln^{13}\alpha_{eq}$	−10.1	−10.1	0.0	−26.7	−26.7	0.0
Atom	$C_{0/5}$	$C_{1/5}$		$C_{0/16}$	$C_{3/6}$	
$\ln^{13}\alpha_{eq}$	–22	–22	0.0	1.1	1.4	0.3
Atom	$C_{0/6}$	$C_{1/6}$		$C_{0/17}$	$C_{4/3}$	
$\ln^{13}\alpha_{eq}$	−17.5	−17.5	0.0	−31.9	−31.6	0.3
Atom	$C_{0/7}$	$C_{1/7}$		$C_{0/18}$	$C_{5/3}$	
$\ln^{13}\alpha_{eq}$	−14.6	−14.8	0.2	−35.5	−35.2	0.3
Atom	$C_{0/8}$	$C_{1/8}$		$C_{0/19}$	$C_{5/4}$	
$\ln^{13}\alpha_{eq}$	−20.9	−20.9	0.0	0.4	0.4	0.0
Atom	$C_{0/9}$	$C_{1/9}$		$C_{0/20}$	$C_{5/5}$	
$\ln^{13}\alpha_{eq}$	−21.2	−21.1	0.1	−31.5	−31.5	0.0
Atom	$C_{0/10}$	$C_{1/10}$		$C_{0/21}$	$C_{5/6}$	
$\ln^{13}\alpha_{eq}$	−35.3	−35.3	0.0	−51.7	−51.7	0.0
Atom	$C_{0/11}$	$C_{2/2}$		Average	Average	
$\ln^{13}\alpha_{eq}$	−35.9	−35.8	0.1	–23.5	–23.4	0.1

4. DISCUSSION

For the three carbon positions (*CH_3–CH_2–CH_2–, CH_3–*CH_2–CH_2–, and –CH_2–*CH_2–CH_2–) in n-propane, the PS $^{13}\beta$ values predicted by force field in literature is 1.1330, 1.1506, and 1.1519, respectively (Galimov and Ivlev, 1973), where the $\ln^{13}\alpha$ of CH_3–*CH_2–CH_2– and –CH_2–*CH_2–CH_2– to *CH_3–CH_2–CH_2– are 15.4‰ and 16.5‰ respectively. In our prediction, the PS $^{13}\beta$ values for the three positions are 1.1377, 1.1541, and 1.1553 respectively, and the two $\ln^{13}\alpha$ values are 14.3‰ and 15.3‰, which are in good agreements with the $^{13}\beta$ values predicted by force field.

Carbons with stronger bond environments have heavier $\ln^{13}\alpha_{eq}$ values. Methyl carbon has only one C–C bond with three C–H bonds. Its $\ln^{13}\alpha_{eq}$ value is the lightest among all carbon positions in normal alkanes, isomeric alkanes, carboxylic acids, and other molecules ($\ln^{13}\alpha_{met(eq)} = -48.9$ to −50.4, Tables 1–4). Methylene carbon has two C–C bonds with two C–H bonds, which has a stronger bond environment than methyl carbon. Thus, methylene carbons are heavier than methyl carbon ($\ln\alpha_{CH_2(eq)} = -33.8$ to −37.4‰, Tables 1–3). Carboxyl carbon has one C–C bond, one C=O bond and one C–O bond, which is in a very strong bond environment. Thus, it is much heavier than other carbon types in carboxylic acids ($\ln^{13}\alpha_{COOH}$

$_{(eq)} = -2.2$ to -2.6‰, Table 2). Among the benzene carbons in aromatic hydrocarbons, C2–C6 carbons have similar $\ln^{13}\alpha_{eq}$ values ($\ln^{13}\alpha_{eq} = -32.6$ to -31.3‰, Table 5), since they are in similar bond environments. The C1 carbon of benzene is connected to one additional carbon of the adjacent functional group. Thus, its $\ln^{13}\alpha_{eq}$ values are heavier than the remaining carbons in benzene ($\ln^{13}\alpha_{eq} = -20.3 \pm 0.1$‰, n = 14, Table 5).

In the test of normal alkanes, the standard deviation for the three carbon positions (*CH_3–CH_2-CH_2–, CH_3–*CH_2–CH_2–, and –CH_2–*CH_2–CH_2–, n = 6) are 0.05‰, 0.04‰, and 0.05‰, respectively. It suggests that PS $^{13}\beta$ values for the three positions in n-pentane are representative for the same positions in all normal alkanes: $\ln^{13}\alpha_{eq} = -50.3$‰ for methyl carbon, $\ln^{13}\alpha_{eq} = -36.0$‰ for methylene carbon adjacent to the terminal methyl, and $\ln^{13}\alpha_{eq} = -35.1$‰ for methylene carbon in between two other methylenes. These values can be used to analyze laboratory-measured Intra-IDs for long-chain alkanes (e.g., Gilbert et al., 2013, 2016b).

For carboxylic acids with increasing cluster size, the influence of the carboxyl on the methyl $^{13}\beta$ value decreases. $\ln^{13}\alpha_{Penta\text{-}Hexa(met)}$ is < 0.2‰ when the carboxyl is three or more methylenes away from the methyl carbon. Similar to the methyl carbon, extending the carbon chain has little influence on the $\ln^{13}\alpha_{carb(eq)}$ value of the carboxyl carbon ($\ln^{13}\alpha_{carb(eq)} = -2.4 \pm 0.15$‰, n = 5). For a target position in an alkane or carboxylic acid, ignoring atoms that are three bonds away from it can provide an accurate estimation of the PS $^{13}\beta$ value in a chain. The molecules with a functional group that is at least three bonds in a chain away from a terminal methyl carbon has similar $\ln^{13}\alpha_{met(eq)}$ values (Table 4), which indicates that to estimate the PS $^{13}\beta_{met}$ value of a methyl position for a methyl carbon with two adjacent methylenes (*CH_3–CH_2–CH_2–R), we can build a butane molecule to represent its bond environment and use the butane PS $^{13}\beta_{met}$ value to represent the PS $^{13}\beta$ value of the methyl carbon in the molecule of concern. The chain molecule examples support that the PS $^{13}\beta$ value of a target position can only be influenced by their proximal three bonds in a chain.

The calculation results of aromatic hydrocarbons show that an adjacent functional group has a significant influence only on the PS $^{13}\beta$ value of the C1 carbon in benzene (standard deviation = 1.0‰, Table 5) but has a negligible influence on the C2–C6 carbons (standard deviations = 0.2‰, Table 5). This finding indicates that to estimate the PS $^{13}\beta$ value of a ring, we can consider only its one adjacent ring or three proximal bonds in a chain. For benzene PS isotope studies, if the C1 position is not the target position, substituting the adjacent functional groups by a methyl group can provide a good approximation for the C2–C6 carbons. If we are working with a PSIA accuracy of 1‰ (e.g., Eiler et al., 2017; Cesar et al., 2019), a benzene cluster with one adjacent ring or three proximal bonds in a chain is sufficiently accurate to estimate its PS $^{13}\beta$ value.

In the cutoff calculation of the CoA molecule, the 5 clusters consider three proximal bonds in a chain and/or one adjacent ring of each carbon position. The comparison between the entire CoA molecule calculation and the cutoff calculation shows that the PS $\ln^{13}\alpha_{eq}$ values estimated by the cutoff calculation are in good agreement with those calculated by considering the entire molecule (absolute differences < 0.3‰). The results suggest that considering three proximal bonds in a chain and/or one adjacent ring of a target position can provide an accurate estimation of PS $^{13}\beta$ values. Such simplification can be expanded from methyl carbon and benzene carbons to other carbon positions. In addition to the PS $^{13}\beta$ value, the compound-specific $^{13}\beta$ value, i.e., the average $^{13}\beta$ value of the whole molecule, between the calculation results from the entire molecule and the five clusters is 0.1‰. Our results indicate that the cutoff calculation can be used to estimate $\ln^{13}\alpha_{eq}$ values for large organic molecules with high accuracy. To estimate the PS $^{13}\beta$ values of adenine, we only need a cluster of an adenine and its adjacent tetrahydrofuran. However, the calculation of tetrahydrofuran must consider both adenine and the $C_5H_{11}O_{13}P_3$ group. Thus, the adenine cluster is not calculated independently. To calculate the vibrational frequencies of $C_{0/10}$ (*C in $C_5H_{11}O_{13}P_3$), the angle of $\angle C_{0/9}$-$C_{0/10}O_{0/21}$ must be maintained. Therefore, sufficient atoms ($C_{0/11}$–$C_{0/14}$, the isobutane) must be located on the other side of the pyrophosphate to keep the angle of $\angle C_{0/9}C_{0/10}$-$O_{0/21}$ from bending. Therefore, cluster 1 is still sufficiently large for computational accuracy. If $C_{0/10}$ is not a target position, the clusters can be further simplified, and the adenine and $C_5H_{11}O_{13}P_3$ clusters can be calculated independently.

The above results show that to estimate a PS $^{13}\beta$ value for a specific carbon position, we can use the cutoff calculation to simplify the calculation to a small cluster, where the target position is surrounded by its proximal three bonds in a chain and/or one adjacent ring on each side. Such simplification not only is useful for estimating PS $^{13}\beta$ values accurately and efficiently but also works for the calculation of KIEs of biochemical reactions that have the solvent effect. Biochemical reactions rarely occur in a gas phase. Therefore, the theoretical calculation of such molecules must consider solvent effects. Surrounding a target molecule with water molecules and/or protein pieces can simulate a solution environment realistically (Rustad et al., 2008, 2010; Zhang and Liu, 2014; He and Liu, 2015). However, the optimization of a large molecule with more than 50 atoms by Gaussian software requires from 10 s to 100 s GB computer memory, which can easily result in frequent convergence failures. Such solvent treatment to a large organic molecule is computationally impracticable. In addition to optimization, a transition-state search for a reaction system with large organic molecules and enzymes is severely restricted by current computational resources. For instance, in the synthesis of fatty acids, one key step is the conversion of pyruvate to acetyl-CoA by a cluster of enzymes. The whole reaction involves 93 atoms without considering enzymes. The transition-state search for such reactions considering the solvent effect is computationally prohibitive. However, if we are studying the KIE of the acetyl carbons in this process, the cutoff calculation can simplify CoA to a small cluster with three proximal bonds to the thiol ($HSCH_2CH_2NH_2$), which can represent the active site. Such a cutoff system involves only 20 atoms. Adding water mole-

cules or protein pieces into the system and the transition-state search for such a reaction is doable.

5. CONCLUSIONS

Benefiting from the recent development of position-specific isotope analysis techniques, Intra-ID has become a promising tool for identifying and quantifying the production and consumption pathways of large molecules. Position-specific β factor can serve as an absolute reference for understanding measured Intra-IDs. The cutoff calculation breaks a large organic molecule down to a set of small clusters where a target atom is surrounded by its most adjacent three bonds in a chain and/or one ring. For large organic molecules, the approach provides accurate PS $^{13}\beta$ value estimations and takes less time than calculating the entire molecule. It is especially useful for KIE calculation for enzymatic reactions with solvent effects and at a higher theoretical level.

Declaration of Competing Interest

The authors declare that they have no known competing financial interests or personal relationships that could have appeared to influence the work reported in this paper.

ACKNOWLEDGMENTS

Boswell Wing and two anonymous reviewers are acknowledged for their constructive comments and suggestions. The project is benefited from comments from XB Cao, YN Zhang, ST Zhang, and Q Liu.

Funding: This work was supported by the National Natural Science Foundation of China [41490635, 41530210]; the strategic priority research program (B), Chinese Academy of Sciences [XDB18010100].

APPENDIX A. SUPPLEMENTARY MATERIAL

Supplementary data to this article can be found online at https://doi.org/10.1016/j.gca.2019.10.032.

REFERENCES

Abelson P. H. and Hoering T. C. (1961) Carbon isotope fractionation in formation of amino acids by photosynthetic organisms. *Proc. Natl. Acad. Sci.* **47**, 623–634.

Anisimov V. and Paneth P. (1999) ISOEFF98. A program for studies of isotope effects using Hessian modifications. *J. Math. Chem.* **26**, 75–86.

ap Rees, T. and Morrell, S. (1990) Carbohydrate metabolism in developing potatoes. Am. J. Potato Res. 67, 835–847.

Bayle K., Gilbert A., Julien M., Yamada K., Silvestre V., Robins R. J., Akoka S., Yoshida N. and Remaud G. S. (2014) Conditions to obtain precise and true measurements of the intramolecular 13 C distribution in organic molecules by isotopic 13 C nuclear magnetic resonance spectrometry. *Anal. Chim. Acta* **846**, 1–7.

Bayle K., Grand M., Chaintreau A., Robins R. J., Fieber W., Sommer H., Akoka S. and Remaud G. r. S. (2015) Internal referencing for 13C position-specific isotope analysis measured by NMR spectrometry. *Anal. Chem.* **87**, 7550–7554.

Becke A. D. (1993) Density-functional thermochemistry. III. The role of exact exchange. *J. Chem. Phys.* **98**, 5648–5652.

Bennet A. J. and Sinnott M. L. (1986) Complete kinetic isotope effect description of transition states for acid-catalyzed hydrolyses of methyl. alpha- and. beta-glucopyranosides. *J. Am. Chem. Soc.* **108**, 7287–7294.

Bigeleisen J. and Mayer M. G. (1947) Calculation of equilibrium constants for isotopic exchange reactions. *J. Chem. Phys.* **15**, 261–267.

Black J. R., Yin Q. Z., Rustad J. R. and Casey W. H. (2007) Magnesium isotopic equilibrium in chlorophylls. *J. Am. Chem. Soc.* **129**, 8690–8691.

Cesar J., Eiler J., Dallas B., Chimiak L. and Grice K. (2019) Isotope heterogeneity in ethyltoluenes from Australian condensates, and their stable carbon site-specific isotope analysis. *Org Geochem.* **135**, 32–37.

Chen X. Y., Berti P. J. and Schramm V. L. (2000a) Ricin A-chain: kinetic isotope effects and transition state structure with stem-loop RNA. *J. Am. Chem. Soc.* **122**, 1609–1617.

Chen X. Y., Berti P. J. and Schramm V. L. (2000b) Transition-state analysis for depurination of DNA by ricin A-chain. *J. Am. Chem. Soc.* **122**, 6527–6534.

Corso T. N. and Brenna J. T. (1997) High-precision position-specific isotope analysis. *Proc. Natl. Acad. Sci.* **94**, 1049–1053.

Diomande D. G., Martineau E., Gilbert A., Nun P., Murata A., Yamada K., Watanabe N., Tea I., Robins R. J. and Yoshida N. (2015) Position-specific isotope analysis of xanthines: a 13C nuclear magnetic resonance method to determine the 13C intramolecular composition at natural abundance. *Anal. Chem.* **87**, 6600–6606.

Eiler J., Cesar J., Chimiak L., Dallas B., Grice K., Griep-Raming J., Juchelka D., Kitchen N., Lloyd M. and Makarov A. (2017) Analysis of molecular isotopic structures at high precision and accuracy by Orbitrap mass spectrometry. *Int. J. Mass Spectrom.* **422**, 126–142.

Eiler, J.M., Clog, M., Lawson, M., Lloyd, M., Piasecki, A., Ponton, C., Xie, H., Lawson, M., Formolo, M.J. and Eiler, J. M. (2018) The isotopic structures of geological organic compounds, From Source to Seep: Geochemical Applications in Hydrocarbon Systems. Geological Society of London.

Fry B., Carter J. F., Yamada K., Yoshida N. and Juchelka D. (2018) Position-specific 13C/12C analysis of amino acid carboxyl groups–automated flow-injection analysis based on reaction with ninhydrin. *Rapid Commun. Mass Spectrom.* **32**, 992–1000.

Galimov E. M. (1985) *The Biological Fractionation of Isotopes*. Academic Press, London.

Galimov E. M. (2004) Phenomenon of life: between equilibrium and non-linearity. *Orig. Life Evol. Biosph.* **34**, 599–613.

Galimov E. M. (2006) Phenomenon of life: Between equilibrium and non-linearity. Origin and principles of evolution. *Geochem. Int.* **44**, S1–S95.

Galimov E. M. and Ivlev A. A. (1973) Thermodynamic isotope effects in organic compounds. I. Carbon isotope effects in straight-chain alkanes. *Russ. J. Phys. Chem.* **47**, 2787–2791 (In Russian).

Gao C., Cao X., Liu Q., Yang Y., Zhang S., He Y., Tang M. and Liu Y. (2018) Theoretical calculation of equilibrium Mg isotope fractionations between minerals and aqueous solutions. *Chem. Geol.* **488**, 62–75.

Gilbert A., Lollar B. S., Musat F., Giunta T., Chen S., Kajimoto Y., Yamada K., Boreham C. J., Yoshida N. and Ueno Y. (2019) Intramolecular isotopic evidence for bacterial oxidation

of propane in subsurface natural gas reservoirs. *Proc. Natl. Acad. Sci.* **116**, 6653–6658.
Gilbert A., Robins R. J., Remaud G. S. and Tcherkez G. G. (2012a) Intramolecular 13C pattern in hexoses from autotrophic and heterotrophic C3 plant tissues. *Proc. Natl. Acad. Sci.* **109**, 18204–18209.
Gilbert A., Silvestre V., Robins R. J. and Remaud G. S. (2009) Accurate quantitative isotopic ^{13}C NMR spectroscopy for the determination of the intramolecular distribution of ^{13}C in glucose at natural abundance. *Anal. Chem.* **81**, 8978–8985.
Gilbert A., Silvestre V., Robins R. J. and Remaud G. S. (2010) Impact of the deuterium isotope effect on the accuracy of 13C NMR measurements of site-specific isotope ratios at natural abundance in glucose. *Anal. Bioanal. Chem.* **398**, 1979–1984.
Gilbert A., Silvestre V., Robins R. J., Remaud G. S. and Tcherkez G. (2012b) Biochemical and physiological determinants of intramolecular isotope patterns in sucrose from C3, C4 and CAM plants accessed by isotopic 13C NMR spectrometry: a viewpoint. *Nat. Prod. Rep.* **29**, 476–486.
Gilbert A., Silvestre V., Robins R. J., Tcherkez G. and Remaud G. S. (2011a) A 13C NMR spectrometric method for the determination of intramolecular δ13C values in fructose from plant sucrose samples. *New Phytol.* **191**, 579–588.
Gilbert A., Silvestre V., Segebarth N., Tcherkez G., Guillou C., Robins R. J., Akoka S. and Remaud G. S. (2011b) The intramolecular 13C-distribution in ethanol reveals the influence of the CO2-fixation pathway and environmental conditions on the site-specific 13C variation in glucose. *Plant, Cell Environ.* **34**, 1104–1112.
Gilbert A., Yamada K., Suda K., Ueno Y. and Yoshida N. (2016a) Measurement of position-specific 13 C isotopic composition of propane at the nanomole level. *Geochim. Cosmochim. Acta* **177**, 205–216.
Gilbert A., Yamada K. and Yoshida N. (2013) Exploration of intramolecular 13 C isotope distribution in long chain n-alkanes (C11–C31) using isotopic 13 C NMR. *Org Geochem.* **62**, 56–61.
Gilbert A., Yamada K. and Yoshida N. (2016b) Evaluation of on-line pyrolysis coupled to isotope ratio mass spectrometry for the determination of position-specific 13 C isotope composition of short chain n-alkanes (C6–C12). *Talanta* **153**, 158–162.
Gleixner G. and Schmidt H. L. (1997) Carbon isotope effects on the fructose-1, 6-bisphosphate aldolase reaction, origin for non-statistical 13C distributions in carbohydrates. *J. Biol. Chem.* **272**, 5382–5387.
Hartshorn S. and Shiner, Jr, V. (1972) Calculation of H/D, 12 C/13 C, and 12 C/14 C fractionation factors from valence force fields derived for a series of simple organic molecules. *J. Am. Chem. Soc.* **94**, 9002–9012.
He H. and Liu Y. (2015) Silicon isotope fractionation during the precipitation of quartz and the adsorption of H4SiO4 (aq) on Fe (III)-oxyhydroxide surfaces. *Chin. J. Geochem.* **34**, 459–468.
He Y., Cao X., Wang J. and Bao H. (2018) Identifying apparent local stable isotope equilibrium in a complex non-equilibrium system. *Rapid Commun. Mass Spectrom.* **32**, 306–310.
Herschbach D. R., Johnston H. S. and Rapp D. (1959) Molecular partition functions in terms of local properties. *J. Chem. Phys.* **31**, 1652–1661.
Igamberdiev A. U. and Kleczkowski L. A. (2009) Metabolic systems maintain stable non-equilibrium via thermodynamic buffering. *BioEssays* **31**, 1091–1099.
Igamberdiev A. U. and Kleczkowski L. A. (2011) Optimization of CO_2 fixation in photosynthetic cells via thermodynamic buffering. *Bio Syst.* **103**, 224–229.
Joubert V., Silvestre V., Grand M., Loquet D., Ladroue V., Besacier F., Akoka S. and Remaud G. S. (2018) Full spectrum isotopic 13C NMR using polarization transfer for position-specific isotope analysis. *Anal. Chem.* **90**, 8692–8699.
Julien M., Nun P., Höhener P., Parinet J., Robins R. J. and Remaud G. S. (2016) Enhanced forensic discrimination of pollutants by position-specific isotope analysis using isotope ratio monitoring by 13C nuclear magnetic resonance spectrometry. *Talanta* **147**, 383–389.
Julien M., Nun P., Robins R. J., Remaud G. r. S., Parinet J. and Höhener P. (2015a) Insights into mechanistic models for evaporation of organic liquids in the environment obtained by position-specific carbon isotope analysis. *Environ. Sci. Technol.* **49**, 12782–12788.
Julien M., Parinet J., Nun P., Bayle K., Höhener P., Robins R. J. and Remaud G. S. (2015b) Fractionation in position-specific isotope composition during vaporization of environmental pollutants measured with isotope ratio monitoring by 13 C nuclear magnetic resonance spectrometry. *Environ. Pollut.* **205**, 299–306.
Lee C., Yang W. and Parr R. G. (1988) Development of the Colle-Salvetti correlation-energy formula into a functional of the electron density. *Phys. Rev. B* **37**, 785.
Li X. and Liu Y. (2011) Equilibrium Se isotope fractionation parameters: a first-principles study. *Earth Planet. Sci. Lett.* **304**, 113–120.
Li X. and Liu Y. (2015) A theoretical model of isotopic fractionation by thermal diffusion and its implementation on silicate melts. *Geochim. Cosmochim. Acta* **154**, 18–27.
Li Y., Zhang L., Xiong Y., Gao S., Yu Z. and Peng P. a. (2018) Determination of position-specific carbon isotope ratios of propane from natural gas. *Org Geochem.* **119**, 11–21.
Liu C., Liu P., McGovern G. P. and Horita J. (2019) Molecular and intramolecular isotope geochemistry of natural gases from the Woodford Shale, Arkoma Basin, Oklahoma. *Geochim. Cosmochim. Acta* **255**, 188–204.
Liu C., McGovern G. P., Liu P., Zhao H. and Horita J. (2018) Position-specific carbon and hydrogen isotopic compositions of propane from natural gases with quantitative NMR. *Chem. Geol.* **491**, 14–26.
Liu Y. and Tossell J. A. (2005) Ab initio molecular orbital calculations for boron isotope fractionations on boric acids and borates. *Geochim. Cosmochim. Acta* **69**, 3995–4006.
Meinschein W., Rinaldi G., Hayes J. and Schoeller D. (1974) Intramolecular isotopic order in biologically produced acetic acid. *Biomedical Mass Spectrometry* **1**, 172–174.
Monson K. and Hayes J. (1980) Biosynthetic control of the natural abundance of Carbon 13 at specific positions within fatty acids in *Escherichia coli*. Evidence regarding the coupling of fatty acid and phospholipid synthesis. *J. Biol. Chem.* **255**, 11435–11441.
Monson K. and Hayes J. (1982) Biosynthetic control of the natural abundance of carbon 13 at specific positions within fatty acids in Saccharomyces cerevisiae. Isotopic fractionation in lipid synthesis as evidence for peroxisomal regulation. *J. Biol. Chem.* **257**, 5568–5575.
Morandini P. (2009) Rethinking metabolic control. *Plant Sci.: Int. J. Exp. Plant Biol.* **176**, 441–451.
Nimmanwudipong T., Gilbert A., Yamada K. and Yoshida N. (2015) Analytical method for simultaneous determination of bulk and intramolecular 13C-isotope compositions of acetic acid. *Rapid Commun. Mass Spectrom.* **29**, 2337–2340.
Oba Y. and Naraoka H. (2006) Site-specific carbon isotope analysis of aromatic carboxylic acids by elemental analysis/pyrolysis/isotope ratio mass spectrometry. *Rapid Commun. Mass Spectrom.* **20**, 3649–3653.
Piasecki A., Sessions A., Lawson M., Ferreira A., Neto E. S. and Eiler J. M. (2016a) Analysis of the site-specific carbon isotope

composition of propane by gas source isotope ratio mass spectrometer. *Geochim. Cosmochim. Acta* **188**, 58–72.
Piasecki A., Sessions A., Lawson M., Ferreira A., Neto E. S., Ellis G. S., Lewan M. D. and Eiler J. M. (2018) Position-specific 13 C distributions within propane from experiments and natural gas samples. *Geochim. Cosmochim. Acta* **220**, 110–124.
Piasecki A., Sessions A., Peterson B. and Eiler J. (2016b) Prediction of equilibrium distributions of isotopologues for methane, ethane and propane using density functional theory. *Geochim. Cosmochim. Acta* **190**, 1–12.
Remaud G. S. and Akoka S. (2017) A review of flavors authentication by position-specific isotope analysis by nuclear magnetic resonance spectrometry: the example of vanillin. *Flavour Fragrance J.* **32**, 77–84.
Rinaldi G., Meinschein W. and Hayes J. (1974) Intramolecular carbon isotopic distribution in biologically produced acetoin. *Biol. Mass Spectrom.* **1**, 415–417.
Robins R. J., Romek K. M., Remaud G. S. and Paneth P. (2017) Non-statistical isotope fractionation as a novel "retro-biosynthetic" approach to understanding alkaloid metabolic pathways. *Phytochem. Lett.* **20**, 499–506.
Romek K. M., Remaud G. S., Silvestre V., Paneth P. and Robins R. J. (2016) Non-statistical 13C fractionation distinguishes coincident and divergent steps in the biosynthesis of the alkaloids nicotine and tropine. *J. Biol. Chem.* **291**, 16620–16629.
Rossmann A., Butzenlechner M. and Schmidt H. L. (1991) Evidence for a nonstatistical carbon isotope distribution in natural glucose. *Plant Physiol.* **96**, 609–614.
Rustad J. R. (2009) Ab initio calculation of the carbon isotope signatures of amino acids. *Org Geochem.* **40**, 720–723.
Rustad J. R., Casey W. H., Yin Q. Z., Bylaska E. J., Felmy A. R., Bogatko S. A., Jackson V. E. and Dixon D. A. (2010) Isotopic fractionation of Mg 2+(aq), Ca 2+(aq), and Fe 2+(aq) with carbonate minerals. *Geochim. Cosmochim. Acta* **74**, 6301–6323.
Rustad J. R., Nelmes S. L., Jackson V. E. and Dixon D. A. (2008) Quantum-chemical calculations of carbon-isotope fractionation in CO2 (g), aqueous carbonate species, and carbonate minerals. *J. Phys. Chem. A* **112**, 542–555.
Savidge W. B. and Blair N. E. (2004) Patterns of intramolecular carbon isotopic heterogeneity within amino acids of autotrophs and heterotrophs. *Oecologia* **139**, 178–189.
Savidge W. B. and Blair N. E. (2005) Intramolecular carbon isotopic composition of monosodium glutamate: biochemical pathways and product source identification. *J. Agric. Food. Chem.* **53**, 197–201.
Sharp T. E. and Johnston H. S. (1962) Hydrogen—deuterium kinetic isotope effect, an experimental and theoretical study over a wide range of temperature. *J. Chem. Phys.* **37**, 1541–1553.
Stern M. J. and Wolfsberg M. (1966a) On the absence of isotope effects in the absence of force constant changes. *J. Chem. Phys.* **45**, 2618–2629.
Stern M. J. and Wolfsberg M. (1966b) Simplified procedure for the theoretical calculation of isotope effects involving large molecules. *J. Chem. Phys.* **45**, 4105–4124.
Suda K., Gilbert A., Yamada K., Yoshida N. and Ueno Y. (2017) Compound–and position–specific carbon isotopic signatures of abiogenic hydrocarbons from on–land serpentinite–hosted Hakuba Happo hot spring in Japan. *Geochim. Cosmochim. Acta* **206**, 201–215.
Świderek K. and Paneth P. (2011) Binding ligands and cofactor to L-lactate dehydrogenase from human skeletal and heart muscles. *J. Phys. Chem. B* **115**, 6366–6376.
Świderek K. and Paneth P. (2012) Extending limits of chlorine kinetic isotope effects. *J. Org. Chem.* **77**, 5120–5124.
Świderek K. and Paneth P. (2013) Binding isotope effects. *Chem. Rev.* **113**, 7851–7879.
Urey H. C. (1947) The thermodynamic properties of isotopic substances. *J. Chem. Soc. (Resumed)*, 562–581.
Wang Y., Sessions A. L., Nielsen R. J. and Goddard, III, W. A. (2009a) Equilibrium 2H/1H fractionations in organic molecules: I. Experimental calibration of ab initio calculations. *Geochim. Cosmochim. Acta* **73**, 7060–7075.
Wang Y., Sessions A. L., Nielsen R. J. and Goddard W. A. (2009b) Equilibrium 2H/1H fractionations in organic molecules. II: Linear alkanes, alkenes, ketones, carboxylic acids, esters, alcohols and ethers. *Geochim. Cosmochim. Acta* **73**, 7076–7086.
Wang Y., Sessions A. L., Nielsen R. J. and Goddard W. A. (2013) Equilibrium 2H/1H fractionation in organic molecules: III. Cyclic ketones and hydrocarbons. *Geochim. Cosmochim. Acta* **107**, 82–95.
Webb M. A. and Miller, III, T. F. (2014) Position-specific and clumped stable isotope studies: comparison of the Urey and path-integral approaches for carbon dioxide, nitrous oxide, methane, and propane. *J. Phys. Chem. A* **118**, 467–474.
Williams, I.H. and Wilson, P.B. (2016) Kinetic isotope effects, in: Tuñón, I., Moliner, V. (Eds.), Simulating Enzyme Reactivity: Computational Methods in Enzyme Catalysis. Royal Society of Chemistry, pp. 150–184.
Wolfsberg M. and Stern M. (1964) Validity of some approximation procedures used in the theoretical calculation of isotope effects. *Pure Appl. Chem.* **8**, 225–242.
Xie H., Ponton C., Formolo M. J., Lawson M., Peterson B. K., Lloyd M. K., Sessions A. L. and Eiler J. M. (2018) Position-specific hydrogen isotope equilibrium in propane. *Geochim. Cosmochim. Acta* **238**, 193–207.
Zhang S. and Liu Y. (2014) Molecular-level mechanisms of quartz dissolution under neutral and alkaline conditions in the presence of electrolytes. *Geochem. J.* **48**, 189–205.
Zhang Y. and Liu Y. (2018) The theory of equilibrium isotope fractionations for gaseous molecules under super-cold conditions. *Geochim. Cosmochim. Acta* **238**, 123–149.

Associate Editor: Ann Pearson